

THE MOLECULAR BEHAVIORS OF CALIXARENES AT THE AIR-WATER INTERFACE: DENSITY FUNCTIONAL THEORY, SURFACE PRESSURE, POTENTIAL, AND EFFECTIVE DIPOLE MOMENT

Faridah Lisa Supian^{1a*}, Wong Yeong Yi^{2a}, Nur Farah Nadia Abd Karim^{3a}, Afiq Radzwan^{4a}, Darvina Lim Choo Kheng^{5a}, Abdullah Faisal Al Naim^{6b}

Abstract: This study examined the behaviors of Langmuir-Blodgett ultrathin calixarene films at the air-water interface. The Langmuir trough was used to estimate the surface pressure, surface potential, and effective dipole moment of two calixarenes, namely, calix[4]arene (THC4) and calix[8]arene (THC8). The band gap was determined using the density functional theory (DFT). The DFT simulation gave a band gap of 2.28 eV for THC4, confirming that THC4 was an insulator. The surface pressure isotherms of THC4 and THC8 yielded the expected molecular behavior from the gaseous to the solid phases. THC4 and THC8 showed a perpendicular and a parallel orientation in the air-water subphase, respectively. The ΔV_{max} values of THC4 and THC8 were 205 mV and 141 mV, respectively, and their μ_{-max} values were 0.147 D and 0.088 D, respectively.

Keywords: Calixarene, density functional theory, effective dipole moment, Langmuir-Blodgett, surface potential

1. Introduction

Nanomaterials are important inventions for many applications, such as nanosensors and drug delivery systems (Azahari et al., 2012; Lim et al., 2020). In particular, the contribution of host-guest nano-molecules, known as calixarenes, encompasses various sectors, including biosensors, healthcare, biomedical, and transport agents in biological systems (Edwards et al., 2021; Kumar et al., 2019; Sanabria Español & Maldonado, 2019). Structurally, calixarenes consist of repeating phenol units linked via alkylidene groups with unique upper rims and basket-like lower rims (Shinkai, 1993). Calixarenes are electrical insulators, and reduced graphene oxide (rGO) enhances the electric conductivity of the non-conductive material (Lim et al., 2020; Al-Rubaye et al., 2017; Echabaane et al., 2013).

The structure and properties of calix[4]arene derivatives and other related guest molecules were studied using the density-functional theory (DFT). These properties included the total interaction energy, electrochemical, and photophysical properties (Ortolan et al., 2018; Sharma et al., 2020). However, studies on the density of state (DOS) and

band gap of calix[4]arene are scarce, if not nonexistent. The band gap is the primary factor determining a material's properties and electrical conductivity (Loa et al., 2018; Wu et al., 2020). Elementary experimental studies of calixarene also are crucial to mimic their potential applications. Also, the surface pressure, surface potential, and effective dipole moment were studied using the Langmuir-Blodgett trough in this work (Azahari et al., 2012).

In this study, the behavior of calix[4]arenes at the air-water interface was investigated using a combination of the theoretical and experimental approaches.

2. Methodology

2.1 The DFT Study of Calixarene

This study investigated two calixarenes, i.e., 25, 26, 27, 28-tetrahydrocalix[4]arene, and 49, 50, 51, 52, 53, 54, 55, 56-octahydrocalix[8]arene. They were abbreviated as THC4 and THC8, respectively. For the theoretical study, quantum ESPRESSO (QE) was used to estimate the DOS and band gap of calixarenes based on their optimized structures (Liao et al., 2021; Woods-Robinson et al., 2020).

DOS was calculated according to the method of first-principle pseudopotential implemented in the QE simulation with the plane-wave as a basis set (Giannozzi et al., 2009). Geometry optimization was performed using the generalized gradient approximation (GGA) in the form of Perdew–Berke–

Authors information:

^aDepartment of Physics, Faculty of Science and Mathematics, Sultan Idris Education University (UPSI), MALAYSIA. E-mail: faridah.lisa@fsmpt.upsi.edu.my¹, wongyeongyi97@gmail.com², farahnadia2512@gmail.com³, afiq@fsmpt.upsi.edu.my⁶, darvinalim@gmail.com⁵

^bDepartment of Physics, College of Science, King Faisal University, SAUDI ARABIA. E-mail: anaim2@kfu.edu.sa

*Corresponding Author: faridah.lisa@fsmpt.upsi.edu.my

Received: April 14, 2022

Accepted: June 23, 2022

Published: October 31, 2022

Erzndof (PBE) as an exchange-correlation function to treat the electron-electron interaction (Lawal et al., 2017; Yazzev et al., 2010). All electron-ion core interactions for C, H, and O atoms were treated using full relativistic norm-conserving pseudopotentials of the standard solid-state pseudopotential library (Dal Corso, 2014) Plane-wave basis sets with kinetic energy cutoffs of 25 Ry and 225 Ry were used for expanding the electron wave functions and charge density, respectively. K-points were generated by the irreducible Brillouin zone sampled with a set of (1, 1, 1) Monkhorst-Pack grid using the Gaussian smearing technique for calculating DOS. The geometry optimization was calculated using the Born-Oppenheimer approximation by determining the cell dimension and atomic positions. Within the adopted numerical approximations, the energy function was minimized using the intrinsic Broyden-Fletcher-Goldfarb-Shanno (BFGS) algorithm until their maximum atomic forces were lower than the threshold of 1.0×10^{-3} Ry/Bohr (Giannozzi et al., 2009). Figure 1 shows the interactive chemical structure for the model of calix[4]arene derived from the crystallographic information file (CIF) in QE.

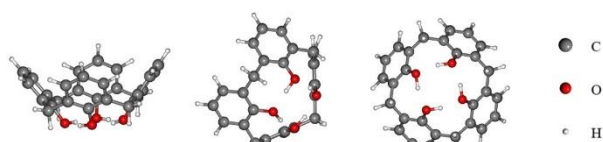


Figure 1. The interactive chemical structure for the model of calix[4]arene in three dimensions.

The contribution of each atom in a structure was quantified based on the valence and conduction band peaks of a DOS curve (Hu & Shang, 2019). Also, the band structure was used to determine the contribution of atoms in the conduction and valence band (Shen et al., 2016). Besides, the structure properties, i.e., whether the structure was a conductor, semiconductor, or insulator, were determined (Kumar et al., 2016).

2.2 Surface Pressure-Area (Π -A), Surface Potential-Area (ΔV -A), and Effective Dipole Moment-Area (μ^+ -A) Isotherms

Experiments of this study were conducted in a 1K cleanroom at room temperature. Calixarenes of 0.2 mg/ml were formed and spread on an air-water subphase. A KSV NIMA 2002 System 2 Langmuir-Blodgett deposition trough attached with a KSV SPOT was used for the experiments. The ΔV -A of the calix[n]arene monolayer was determined using the vibrating plate capacitor method with the KSV SPOT probe at a sensitivity of 1 mV. Deionized water with a resistivity of 18.2 M Ω .cm was gently put into the trough with the surface pressure monitored and stabilized at 25 °C.

The monolayer was then compressed symmetrically with two hydrophilic barriers at 12 mm/min. At the onset of the compression, both Π -A and ΔV -A isotherms were performed

simultaneously using the KSV. Extrapolating Π -A isotherm graph yielded the mean molecular area for THC4 and THC8. Therefore, their experimental radius was calculated using the formula for computing the area of a circle.

The surface potential-area (ΔV -A) value of the calixarene monolayer was obtained simultaneously during the Π -A isotherm experiment. Further assessment of ΔV -A values was induced to the average effective dipole moment (μ^+) by the Helmholtz equation (Azahari et al., 2012).

3. Results and Discussions

3.1 The DFT study

The total DOS (TDOS) and partial DOS (PDOS) were calculated to elucidate the band characteristics of THC4 (Radzwan et al., 2020). Figure 2 below shows each atom's TDOS and PDOS. The Fermi energy was -3.346 eV and located in the band gap, confirming that THC4 was an insulator (Jin et al., 2021; Khazaei et al., 2016). The C atom gave the highest contribution in both valences (p) and conduction bands (x) compared to O (valence q; conduction bands y) and H (valence r; conduction bands z). The O atoms gave nearly the same contribution as the H atoms in the valence band while showing the lowest contribution in the conduction band. Overall, C atoms contributed to the band gap. This finding agreed with Gillespie and Martinsovich (2019) and Wu et al. (2021). The dominance of C atoms in DOS was due to its unique electron configuration (Wu et al., 2020).

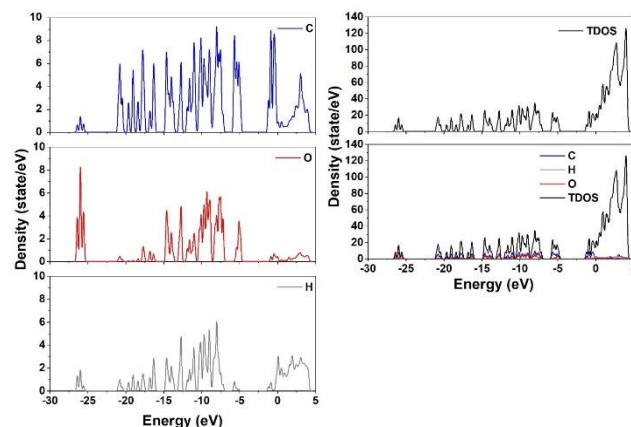


Figure 2. DOS versus the energy of carbon, oxygen, hydrogen, TDOS, and PDOS.

The band gap is 2.28 eV (As in Table 1). However, the band structure based on the PBE exchange-correlation potential underestimated the band gap of insulating materials (Morales-García et al., 2017). With PBE treatment, the actual THC4 band gap should be higher than this computed value. Table 1 shows the bandgap values of calixarenes from other studies. These derivatives were widely used in different applications, such as the fabrication of organic light-emitting diodes, organic optoelectronic

devices, solar cells, photocatalysts, and thermistors (Leontie et al., 2018; Sharma et al., 2020; Wang et al., 2020). Meanwhile, the conductivity, the threshold of 3.0 eV was used to estimate the conductivity of THC4 (Wu et al., 2020).

Table 1. Band gap values of several calix[4]arenes derivatives.

Nanomaterials	Band gap (eV)	References
25, 26, 27, 28-tetrahydrocalix[4]arene (THC4)	2.280	This study
p-tert-butyl-calix[4]arene	3.581	(Sharma et al., 2020)
	3.582	
	3.583	
	3.594	
tertbutylcalix[4]arene with propargyl bromide	1.850	(Leontie et al., 2018)
	2.640	
	2.770	
	3.650	
Thiacalix[4]arene-Protected Titanium-oxo	2.190	(Wang et al., 2020)
	2.240	

3.2 Studies of Π -A, ΔV -A, and μ -A Isotherm for THC4 and THC8

Figure 3 shows the Π -A isotherms of TCH4 and TCH8. As the volume of the solution increased, THC isotherms shifted gradually to the right-hand side (Figure 3a) while the THC8 curves remained nearly the same. The intermolecular packing structures between these two calixarenes might have caused their different isothermic behaviors (Dhanabalan et al., 1999).

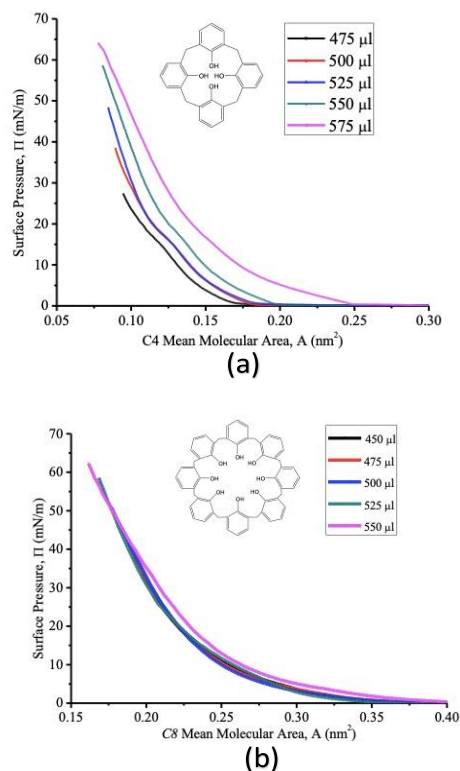


Figure 3. Π -A isotherms: (a) THC4 and b) THC8.

The calixarene molecules moved closer to each other when barriers were shifted to reduce the trough area, changing the surface pressure substantially. Besides, the isotherms of THC4 and THC8 showed the same smooth pattern of phase transition. The molecular transition from the gaseous to liquid, and later, solid phases, showed no flexure before achieving the highest possible surface pressure. Eventually, these phases overlapped into the three-dimensional structure and collapsed.

Table 2. The Π -A isotherms of the Langmuir monolayer for calixarenes.

The Langmuir monolayer	Mean molecular area (nm ²)	Radius (nm)	Orientation at the air-water subphase
THC4	0.135	0.207	Parallel
	0.134	0.207	
	0.127	0.201	
	0.139	0.210	
	0.157	0.224	
THC8	0.251	0.283	Perpendicular
	0.237	0.275	
	0.242	0.278	
	0.232	0.272	
	0.250	0.282	

Table 2 shows the experimental mean molecular area, radius, and the possible orientations of THC4 and THC8 ring against the water surface plane. The experimental mean molecular area of THC4 was smaller than THC8 by nearly half since THC4 comprised four phenolic units while THC8 was

eight. Therefore, the optimal mean molecular area and radius for THC4 were 0.13 nm² and 0.21 nm, respectively. The optimal mean molecular area and radius for THC8 were 0.24 nm² and 0.27 nm, respectively.

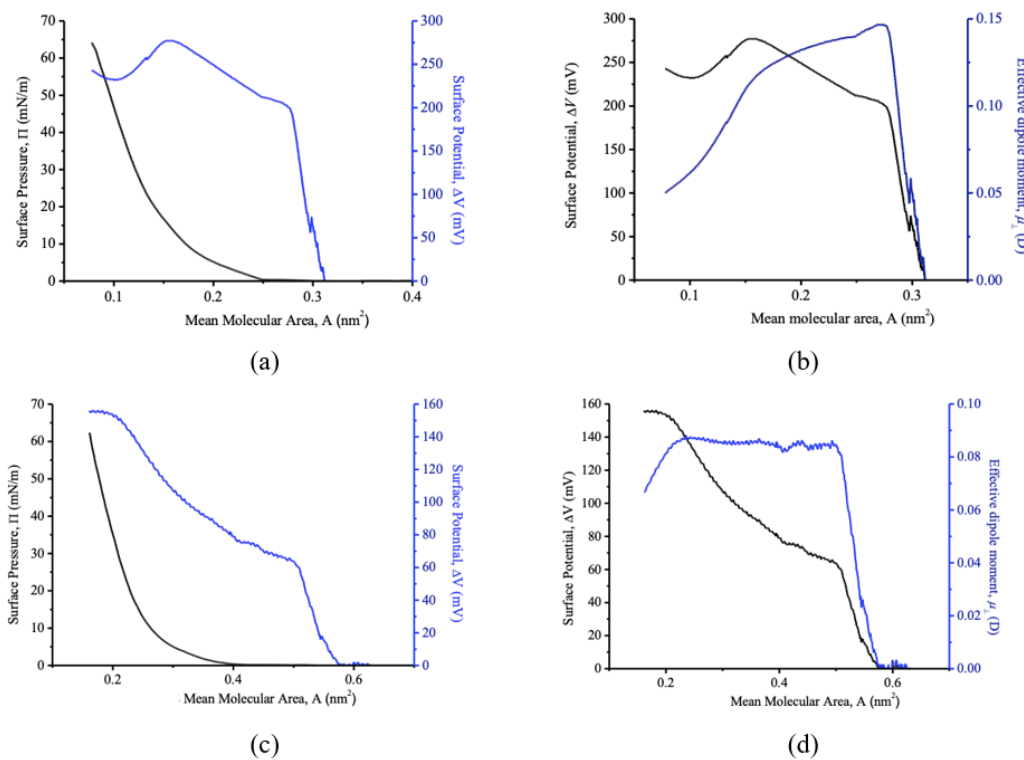


Figure 4. (a) The Π -A isotherm and ΔV -A of THC4, (b) the μ -A isotherm of THC4, (c) the Π -A isotherm and ΔV -A of THC8, and (d) the μ -A isotherm of THC8.

Figure 4 compares the Π -A, ΔV -A, and μ -A isotherms THC4 THC8. ΔV values increased at 0.31 nm² before Π increased at 0.25 nm² (Figure 4a) with the ongoing compression because the molecules began rearranging themselves. Flexures occurred in the ΔV and μ when THC4 changed from the gaseous to the liquid phase at 15 mN/m, coinciding with the sudden rapid increase in Π at 0.15 nm². Another flexure occurred at 0.27 nm² because the molecules aligned themselves, arranging in a uniform gaseous state. However, the μ started to decline from 0.27 nm² onward when the molecular area decreased.

Figures 4c and 4d show the Π -A, ΔV -A, and μ -A isotherms of THC8. Similar to THC4, the ΔV values of THC8 also showed the same increasing pattern. Specifically, the ΔV values of THC8 increased first at 0.57 nm² before Π escalated at 0.40 nm². An obvious flexure occurred in the ΔV -A curve at 0.50 nm², indicating that the THC8 molecules changed into the better-arranged gaseous phase. A sudden change also happened in the μ -A isotherm of THC8. When the THC8 molecules transformed into the liquid phase, minor flexure occurred in the ΔV -A curve at 0.40 nm². The μ of THC8 remained nearly constant, starting from the point at 0.23

nm² to 0.5 nm² when the THC8 molecules went through a substantially greater alignment before 0.5 nm². Thus, after the 0.5 nm², the molecules improved their alignment slightly with little changes in the μ^+ throughout the entire compression (Supian, 2010). Thus, 30 mN/m was the selected surface pressure for depositing calixarene on the substrate because the three calixarenes existed in the solid phase.

Table 3 shows the maximum ΔV (ΔV_{\max}) of THC4 and THC8 based on the maximum μ^+ (μ^+_{\max}) on the isotherms. These data were the results of the arrangement, orientation, and interaction among the calixarene molecules.

Table 3. The maximum ΔV (ΔV_{\max}) of THC4 and THC8 based on ΔV -A and μ^+ -A isotherms.

Calixarenes	Volume (μ l)	ΔV_{\max} (mV)	μ^+_{\max} (D)
THC4	575	205	0.147
THC8	550	141	0.088

4. Conclusion

This study investigated the behavior of Langmuir-Blodgett ultrathin films at the air-water interface for two calixarenes, namely calix[4]arene and calix[8]arene. The DFT study estimated the band gap as 2.28 eV based on the DOS calculation. The Fermi energy in the band gap verified that the calixarene was an insulator. Π -A isotherms were formed. THC4 and THC8 showed a perpendicular and a parallel orientation in the air-water subphase, respectively. ΔV_{\max} values of TCH4 and THC8 were 205 mV and 141mV, respectively, and their μ^+_{\max} values were 0.147 D and 0.088 D, respectively.

5. Acknowledgements

The Ministry of Education of Malaysia supported this study under the Fundamental Research Grants Scheme 2020-0256-103-02 (FRGS/1/2020/STG07/UPSI/02/2). The authors thank Sultan Idris Education University (UPSI) for managing the grants and all parties involved directly or indirectly for recommendations and assistance for this study.

6. References

- Al-Rubaye, S., Rajagopalan, R., Dou, S. X. & Cheng, Z. (2017). Facile synthesis of a reduced graphene oxide wrapped porous NiCo₂O₄ composite with superior performance as an electrode material for supercapacitors. *Journal of Materials Chemistry A*, 5(36), 18989-18997.
- Azahari, N. A., Supian, F. L. & Malik, S. A. (2012). Interaction Between Langmuir Films Of Calix [4] Arenes With Aqueous Lead Ions.
- Dal Corso, A. (2014). Pseudopotentials periodic table: From H to Pu. *Computational Materials Science*, 95, 337-350.
- Dhanabalan, A., Gaffo, L., Barros, A. M., Moreira, W. C. & Oliveira, O. N. (1999). Surface pressure and surface potential isotherms of ytterbium bisphthalocyanine Langmuir monolayers. *Langmuir*, 15(11), 3944-3949.
- Echabaane, M., Rouis, A., Bonnamour, I. & Ouada, H. B. (2013). Optical, electrical and sensing properties of β -ketoimine calix [4] arene thin films. *Materials Chemistry and Physics*, 141(2-3), 781-789.
- Edwards, N. Y., Schnable, D. M., Gearba-Dolocan, I. R. & Strubhar, J. L. (2021). Terpyridine-Functionalized Calixarenes: Synthesis, Characterization and Anion Sensing Applications. *Molecules*, 26(1), 87.
- Giannozzi, P., Baroni, S., Bonini, N., Calandra, M., Car, R., Cavazzoni, C., ... & Wentzcovitch, R. M. (2009). QUANTUM ESPRESSO: a modular and open-source software project for quantum simulations of materials. *Journal of physics: Condensed matter*, 21(39), 395502.
- Gillespie, P. N. & Martsinovich, N. (2019). Origin of charge trapping in TiO₂/reduced graphene oxide photocatalytic composites: Insights from theory. *ACS applied materials & interfaces*, 11(35), 31909-31922.
- Hu, R. & Shang, J. (2019). Quantum capacitance of transition metal and nitrogen co-doped graphenes as supercapacitors electrodes: A DFT study. *Applied Surface Science*, 496, 143659.
- Jin, K. H., Yeom, H. W. & Liu, F. (2020). Doping-induced topological phase transition in Bi: The role of quantum electronic stress. *Physical Review B*, 101(3), 035111.
- Karmakar, A., Karthick, K., Sankar, S. S., Kumaravel, S., Madhu, R. & Kundu, S. (2021). A vast exploration of improvising synthetic strategies for enhancing the OER kinetics of LDH structures: a review. *Journal of Materials Chemistry A*, 9(3), 1314-1352.
- Khazaei, M., Ranjbar, A., Arai, M. & Yunoki, S. (2016). Topological insulators in the ordered double transition metals M₂'M''C₂MXenes (M'= Mo, W; M''= Ti, Zr, Hf). *Physical Review B*, 94(12), 125152.
- Kumar, A., Balasubramaniam, K. R., Kangsabanik, J. & Alam, A. (2016). Crystal structure, stability, and optoelectronic properties of the organic-inorganic wide-band-gap

- perovskite CH₃NH₃Bal₃: candidate for transparent conductor applications. *Physical Review B*, 94(18), 180105.
- Kumar, R., Sharma, A., Singh, H., Suating, P., Kim, H. S., Sunwoo, K., ... & Kim, J. S. (2019). Revisiting fluorescent calixarenes: from molecular sensors to smart materials. *Chemical reviews*, 119(16), 9657-9721.
- Lawal, A., Shaari, A., Ahmed, R. & Jarkoni, N. (2017). First-principles investigations of electron-hole inclusion effects on optoelectronic properties of Bi₂Te₃, a topological insulator for broadband photodetector. *Physica B: Condensed Matter*, 520, 69-75.
- Leontie, L., Danac, R., Carlescu, A., Doroftei, C., Rusu, G. G., Tiron, V., ... & Susu, O. (2018). Electric and optical properties of some new functional lower-rim-substituted calixarene derivatives in thin films. *Applied Physics A*, 124(5), 1-12.
- Liao, Y., Peng, R., Peng, S., Zeng, W. & Zhou, Q. (2021). The adsorption of H₂ and C₂H₂ on Ge-doped and Cr-doped graphene structures: A DFT study. *Nanomaterials*, 11(1), 231.
- Lim, D. C., Supian, F. L. & Hamzah, Y. (2020). Langmuir, Raman, and electrical properties comparison of calixarene and calixarene-rGO using Langmuir Blodgett (LB) technique. *Journal of Materials Science: Materials in Electronics*, 31(21), 18487-18494.
- Loa, I., Popuri, S. R., Fortes, A. D. & Bos, J. W. G. (2018). Critical mode and band-gap-controlled bipolar thermoelectric properties of SnSe. *Physical Review Materials*, 2(8), 085405.
- Morales-García, Á., Valero, R. & Illas, F. (2017). An empirical, yet practical way to predict the band gap in solids by using density functional band structure calculations. *The Journal of Physical Chemistry C*, 121(34), 18862-18866.
- Ortolan, A. O., Øestrøm, I., Caramori, G. F., Parreira, R. L., Munoz-Castro, A. & Bickelhaupt, F. M. (2018). Anion recognition by organometallic calixarenes: analysis from relativistic DFT calculations. *Organometallics*, 37(13), 2167-2176.
- Radzwan, A., Lawal, A., Shaari, A., Chiromawa, I. M., Ahams, S. T. & Ahmed, R. (2020). First-principles calculations of structural, electronic, and optical properties for Ni-doped Sb₂S₃. *Computational Condensed Matter*, 24, e00477.
- Sanabria Español, E. & Maldonado, M. (2019). Host-guest recognition of pesticides by calixarenes. *Critical reviews in analytical chemistry*, 49(5), 383-394.
- Shah, A. (2020). A novel electrochemical nanosensor for the simultaneous sensing of two toxic food dyes. *ACS omega*, 5(11), 6187-6193.
- Sharma, V. S., Sharma, A. S., Worthington, S. J., Shah, P. A. & Shrivastav, P. S. (2020). Columnar self-assembly, electrochemical and luminescence properties of basket-shaped liquid crystalline derivatives of Schiff-base-moulded p-tert-butyl-calix [4] arene. *New Journal of Chemistry*, 44(47), 20610-20619.
- Shen, J., Chen, Z., Zheng, L., Li, W. & Pei, Y. (2016). Single parabolic band behavior of thermoelectric p-type CuGaTe₂. *Journal of Materials Chemistry C*, 4(1), 209-214.
- Shinkai, S. (1993). Calixarenes-the third generation of supramolecules. *Tetrahedron*, 49(40), 8933-8968.
- Supian, F.L. (2010). Sensing interactions within nanoscale calixarene and polysiloxane Langmuir-Blodgett films (Doctoral dissertation, The University of Sheffield).
- Wang, X., Yu, Y., Wang, Z., Zheng, J., Bi, Y. & Zheng, Z. (2020). Thiocalix [4] arene-Protected Titanium-Oxo Clusters: Influence of Ligand Conformation and Ti-S Coordination on the Visible-Light Photocatalytic Hydrogen Production. *Inorganic chemistry*, 59(10), 7150-7157.
- Woods-Robinson, R., Han, Y., Zhang, H., Ablekim, T., Khan, I., Persson, K. A. & Zakutayev, A. (2020). Wide band gap chalcogenide semiconductors. *Chemical reviews*, 120(9), 4007-4055.
- Wu, B., Zhang, L., Jiang, B., Li, Q., Tian, C., Xie, Y., ... & Fu, H. (2021). Ultrathin porous carbon nitride bundles with an adjustable energy band structure toward simultaneous solar photocatalytic water splitting and selective phenylcarbinol oxidation. *Angewandte Chemie International Edition*, 60(9), 4815-4822.
- Wu, W., Gong, S. & Sun, Q. (2020). Electronic band structure phase diagram of 3D carbon allotropes from machine learning. *Diamond and Related Materials*, 108, 107990.
- Yazyev, O. V., Moore, J. E. & Louie, S. G. (2010). Spin polarization and transport of surface states in the topological insulators Bi₂Se₃ and Bi₂Te₃ from first principles. *Physical review letters*, 105(26), 266806.